Material Strength and Applied Mechanics
A. Khotsianovsky and Y. Chen (Eds.)
© 2024 The Authors.
This article is published online with Open Access by IOS Press and distributed under the terms
of the Creative Commons Attribution Non-Commercial License 4.0 (CC BY-NC 4.0).
doi:10.3233/ATDE240544

Development of Injection Moulded Electromagnetic Pulse Shielded Polymer Cover

Gábor DOGOSSY[a,1] and Ferenc RONKAY[b]
[a] *Széchenyi István University, Department of Materials Science and Engineering, H-9026 Győr, Egyetem tér 1., Hungary*
[b] *John von Neumann University, Department of Innovative Vehicles and Materials, H-6000 Kecskemét, Izsáki út 10., Hungary*
ORCiD ID: Gábor Dogossy https://orcid.org/0000-0003-2907-0734
Ferenc Ronkay https://orcid.org/0000-0003-0525-1493

Abstract. Technology for an electromagnetic pulse shielded injection moulded product was developed, using in-mould metal mesh and a 3D printed spacer made of the same type of acrylonitrile-butadiene-styrene as the injection moulded polymer. The functional and mechanical properties of the manufactured flat and dumbbel specimens were tested. The metal mesh increased the stiffness of the plastic, decreased its Charpy impact strength, and did not significantly affect its tensile strength. Computed tomography scans confirmed that delamination and microcracking occur during the failure due to different elongation of the plastic and metal. The attenuation at 1 GHz was 16-19 dB, depending on the metal mesh used. The shielding properties were affected by the fact that the high pressure at the mould filling during the injection moulding process distorted the geometry of the metal mesh.

Keywords. Electromagnetic pulse (EMP), shielding effectiveness, polymer cover, mechanical properties, polymer/metal mesh composite

1. Introduction

Nowadays, warfare has undergone major changes. In addition to traditional warfare, electronic warfare is increasingly being used by opposing sides. This method can be used effectively when there is a conflict between developed countries. In recent decades, there have been several wars, such as in Iraq, Afghanistan or African countries, where these methods have not been effective due to the lack of infrastructure [1]. In the case of developed countries, where information technology is pervasive in all infrastructures, electronic warfare tools can cause serious damage. These can range from simple disinformation dissemination, to hacking into enemy territory's IT systems and disabling them. The latter can even be carried out remotely using directed energy weapons [2].

Directed-energy weapons emit energy in the selected direction to produce different effects on the target [3]. These weapons can be divided into the following groups, based

[1] Corresponding Author: Gábor Dogossy, E-mail: dogossy@ga.sze.hu.

on their mechanism of action: acoustic, radio frequency, electromagnetic, laser, microwave, and particle weapons.

The earth, and with it us and our technology, is enveloped in a magnetic field, and disturbances in this magnetic field, which can be caused by an electromagnetic pulse (EMP), can damage or destroy electrical systems [4, 5]. EMPs can be natural, originating from the sun [6], or artificial, resulting from, for example, the explosion of a nuclear bomb [7].

In addition to EMPs from nuclear bombs, there are now smaller weapons, ranging from hand-held size to the JOLT generator (a highly directed, very intense, pulse-like radiator weapon) that can be placed on a small truck, which can be deployed even when parked next to the data centre under attack [8].

EMP protection is relatively simple to implement, using the so-called Faraday cage. This is called shielding, and was first demonstrated in 1823 by the experimental physicist Michael Faraday. The part of the space surrounded by the metal mesh he created eliminates the electromagnetic effect, as the protective effect of the metal mesh prevents the penetration of the external electric field [9]. This type of protection can be used to protect large spaces, even buildings (full shielding). Such a solution is offered by Holland Shielding Systems for the protection of data centres [8], while a simpler and cheaper solution has been developed by researchers at the University of Nebraska, using a special conductive concrete mix (containing finely ground megnetite) that creates the Faraday cage itself [10]. In many cases, there may also be a need for protection of smaller equipment, even portable equipment (local shielding), for which there are several options, including antenna protection, power cable protection or surge protection, which are also found in most households and are primarily intended to protect against lightning strikes, but can also protect against EMP attack to some extent [11].

Kim et al. [12] developed decision factors for classifying electromagnetic pulse (EMP) protection levels and determining different protection measures. Three EMP protection levels were proposed: 80, 60 and 40 dB attenuation, taking into account the characteristics of military equipment and the factors determining the EMP protection level. It is concluded that lightweight protection facilities can replace conventional heavy and robust facilities.

Based on this result, in another work Kim et al. [13], addressed the development of a tactical EMP tent that could enable the protection of mobile electronic devices in the event of an EMP attack. They investigated tents made of metallic fibres (silver, copper, nickel) embedded in fabric materials. The shielding performance of each material was measured in the 30 MHz-1.5 GHz frequency band using the ASTM-D-4935-10 standard. Based on tests, the development of a lightweight EMP shielding facility was found to be feasible.

Recently, the use of polymer matrix composites in the field of EMP shielding has been increasing due to their improved mobility and thus their more flexible application. The conductive component provides shielding, while the polymer matrix provides light weight, chemical and corrosion resistance [14]. The conductive component can be graphene, carbon nanotubes, silver particles, metal mesh or a combination of these [15].

Morales at al [16] investigated with simulation the EMP shielding effectiveness of the carbon-fibre-reinforced-polymer (CFRP) laminate with additional Cu mesh layer. They found that the SE was improved over a wider frequency range by incorporating a component that shields primarily by reflection loss (the Cu mesh) and a component that shields primarily by absorption loss (the CFRP).

The aim of this paper is to develop a polymer/metal mesh composite material that can be used for the production of injection moulded cover materials, providing the appropriate EMP protection for the devices.

2. Materials and methods

2.1. Materials

Acrylonitrile butadiene styrene (ABS), one of the most widely used engineering plastics [17, 18], was chosen as the raw material for the device cover due to its good impact resistance. The specific type was Terluran GP-35 (Resinex). In terms of shielding against magnetic and electric waves, good electrical conductivity and low magnetic permeability are the most important. Therefore, the choice was made for the V4A series of woven stainless steel, marketed by Y Shield, for the protection against high-frequency radiation (HF) and low-frequency electric fields (LF). The shielding determined by the grid size is a function of the wavelength used in the EMP attack, so two types of metal mesh were investigated. V4A10 (marked “A”) is a finely woven, noncorrosive stainless-steel mesh. The attenuation on 1GHz frequency is 40 dB in one-layer according to manufacturer. The mesh width is 1 mm, the wire diameter is 160 µm and the woven thickness is 320 µm. V4A03 (marked “B”) is an extremely fine woven, noncorrosive stainless-steel gauze. The attenuation on 1GHz frequency is 55 dB in one-layer according to manufacturer. The mesh width is 0.3 mm, the wire diameter is 80 µm the woven thickness is 160 µm. For the positioning of the metal mesh fused deposition modeling (FDM) 3D printed grids were used, using Fillamentum PLA Extrafill Natural and Fillamentum PLA Extrafill Traffic Black, of which a spacer grid was printed at a nozzle temperature of 200 °C, a table temperature of 50 °C and a thickness of 0.4 mm with 50% fill.

2.2. Production of specimens

For the determination of mechanical properties, dumbbel specimens (according to ISO 3167A) were first moulded from the unreinforced ABS material. The composite specimens were then produced according to literatures [19, 20]. During the process the 3D printed spacer grid mesh and the metal mesh were inserted into the core side of mould in one layer the fixing with double-sided tapes were solved. The ABS was then injection moulded into the mould cavity onto the pre-inserted structures. In composite systems manufactured using this technique, the metal mesh has been completely retained inside the product (Figure 1). The ABS was dried in a dry air tower at 80°C for 6 hours before processing. The production was carried out on an Arburg Allrounder 420C Golden Edition injection moulding machine with a mould temperature of 40°C, a nozzle temperature of 220°C, a clamping force of 700 kN and an injection speed of 50 cm^3/s. Injection moulding was performed in a two-cavity dumbbell specimen mould.

To measure the attenuation of the shielding, the dumbell specimens were not of suitable geometry, so for this purpose, 2 mm thick 60x60 mm flat specimens were produced in a two-cavity mould, in one of the cavities of which a printed grid and metal mesh were inserted. Injection moulding was carried out on a Mitsubishi MAC VIIIt controlled machine with a mould temperature of 60°C, a nozzle temperature of 240°C and an injection speed of 50 mm/s. During the experiment, 2 different samples were produced with the two types of metal meshes in addition to the reference. The sample containing the metal mesh type V4A10-90 and the 0.4 mm thick printed grid mesh was marked 24A, while the sample containing the metal mesh type V4A03-90 and the 0.4 mm thick printed grid mesh was marked 24B.

Figure 1. Injection moulded dumbbell specimens from the rear.

2.3. Test methods

The tensile properties were tested according to ISO 527 on a computer-controlled INSTRON 5582 universal tensile testing machine. Test speeds of 20 mm/min and clamping lengths of 100 mm were used to test the specimens. From the recorded force-displacement curve, tensile strength (σ_T), the corresponding specific elongation (ε_T) tensile modulus of elasticity (E_T) were determined.

Charpy measurements were performed using a CEAST 6545,000 impact tester according to ISO 179 on unnotched specimens. A 15 J pendulum with a 64 mm support distance was used for the tests. From the test results, the specific energy of fracture (a_C) was calculated.

Mechanical tests were carried out on 5-5 test specimens at room temperature, and the results were used to determine the mean and standard deviation of the respective properties.

The morphological structure of the manufactured specimens was examined by YXLON Y.CT Modular Industrial Computed Tomography (CT) scanner with flat panel.

The effectiveness of the shielding against electromagnetic pulse was measured according to the IEEE-299 standard in the anechoic chamber of the radio frequency laboratory at the Széchenyi István University. During the measurement, signals between 260 MHz and 18 GHz were transmitted on one side of the test object using a transmitter, while the other, shielded side was used to measure the signals transmitted through the test object using a receiver. The difference between the two signals gave the shielding efficiency, which was determined using Eq. (1) [21].

$$SE_{dB} = 20Log_{10}\left[\frac{S_i}{S_t}\right] \text{[dB]}, \tag{1}$$

where SE_{dB} [dB] is shielding effectiveness of the sample, S_i is power flux density on the transmit antenna, S_t is power flux density on the receive antenna.

3. Results and discussions

3.1. Mechanical properties

The tensile test results are shown in Figure 2 and Table 1. The strength results of the ABS used as a reference showed good agreement with the values reported in the technical data sheet. In all cases, an increase in stiffness was observed for the composites. The specimen with thicker metal mesh (24A) showed a better increase in tensile modulus than the specimen with thinner metal mesh (24B). The variation of tensile strength within the standard deviation field does not show significant differences. The two types of metal mesh reduced the specific elongation associated with tensile strength by the same proportion, but elongation at break occurred sooner for the thinner metal mesh in all cases, as can be seen from the curves. The tensile curves of the specimen with the thinner metal mesh (24B) decrease stepwise after the maximum force (Figure 2).

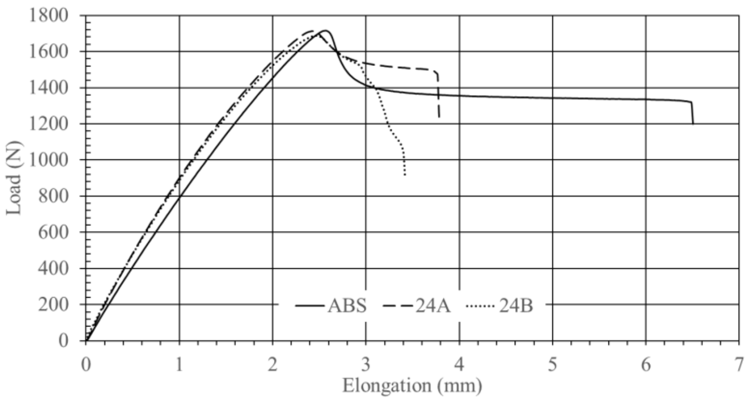

Figure 2. Typical tensile test curves of the samples.

Table 1. Tensile test results of the samples.

		ABS	24A	24B
E	**GPa**	2.03±0.09	2.37±0.11	2.25±0.11
σ_T	**MPa**	42.90±3.6	43.50±4.0	42.40±4.1
ε_T	**%**	2.57±0.08	2.43±0.17	2.47±0.13

In order to find out the reason for this, the tested samples were examined by CT scan and the images are shown in Figure 3. Whitened bands appeared near the fracture surface, which started from the metal mesh and progressed towards the other side of the specimen (Figure 3a). Stress whitening in tensile loading of polymers typically occurs at the stress-retaining sites at the onset of failure, typically associated with the formation of microcracks [22, 23]. CT scans clearly showed a partial delamination between the metal mesh and the moulded ABS (Figure 3b). The delamination is mainly observed in the centre of the sample (Figure 3c). During manufacture, the high injection pressure has wavied the metal mesh and its straightening during tensile load can cause delamination (Figure 3d). It is also clear that the whitening occurred in areas where there was no delamination. This suggests that transverse microcracks in the matrix occurred due to the deformation of the metal mesh during the tensile test. The shape of the delamination suggests that at the end of the tensile test, on the side without the metal mesh, the ABS was able to recover due to elastic deformation, but this was prevented by the metal mesh on the other side (Figure 3a).

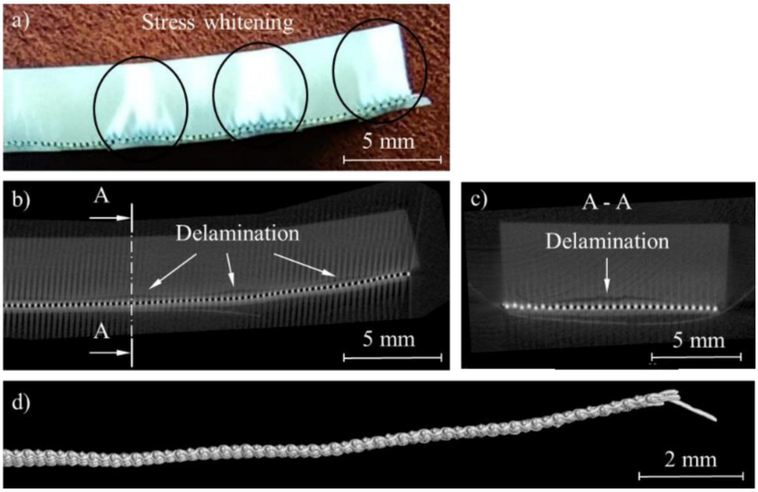

Figure 3. The 24B dumbell specimen after tensile test a) side-view photo b) longitudinal-section CT image c) cross-section CT image d) side-view CT image of metal mesh.

The results of the Charpy impact test are shown in Figure 4. The reference ABS achieved an impact strength close to the technical data sheet of 103 kJ/m^2, but the use of both metal meshes drastically reduced this value. Although there is a slight difference in the mean value between the two metal meshes, the difference was within the range of the standard deviation field and therefore not significant. Such a change could have occurred because there was no proper adhesion between the metal mesh and the matrix, and therefore the metal mesh acted as a stress concentration place, which could have been the origin of the failure.

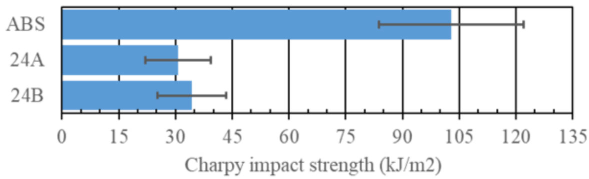

Figure 4. Charpy impact test results of the samples

3.2. Measure of shielding effectiveness

The characteristic curves of the measured shielding effectiveness over the investigated range are shown in Figure 5. The measured values are fluctuating, so linear trend lines were taken for the evaluation and their deviation was investigated. The reference ABS showed no appreciable attenuation over the frequency range investigated. The thicker mesh (24A) shows a decreasing attenuation with increasing frequency, 16 dB attenuation was measured at 1 GHz. The thinner mesh (24B) shows increasing attenuation with increasing frequency, with 19 dB attenuation measured at 1 GHz. While this is better than the attenuation of the other metal mesh, it is not as much as would be expected. However, neither of them meets military requirements, where the lowest attenuation should be 40 dB and the highest 80 dB. A detail of the CT scan of the flat specimen is shown in Figure 6. It is clearly visible that the mesh was deformed during the injection moulding process, which may have contributed to the lower than required attenuation.

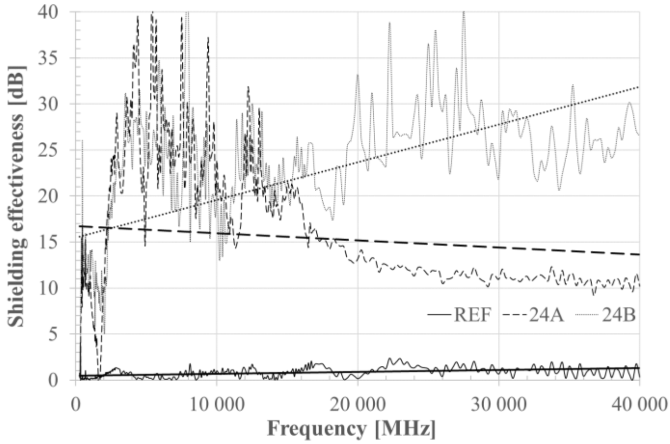

Figure 5. Variation of shielding effectiveness in different samples between 260 MHz and 1 GHz range.

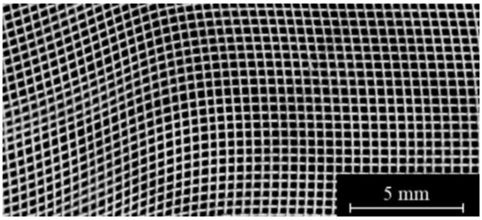

Figure 6. The metal mesh distortion on the CT image from 24B flat specimen.

4. Conclusions

In the development we have produced EMP-shielded polymer composites by injection moulding, which can be used to make covers for household or military equipment. The shielding was provided by a conductive metal mesh, the location of which within the polymer matrix was ensured by a 3D printed spacer grid. Mechanical tests showed that that the properties of the manufactured composites differ from those of ABS, improving under static loads and deteriorating under dynamic loads, but they can still be used as cover materials. As a result of the research, the protection required in everyday use has been achieved in the field of localised shielding, with a lower mass than in the literature [21]. However, further research is needed to achieve military requirements. In the following, we see two areas where there is potential for increasing attenuation and compensating for the resulting increase in weight: the use of multilayer metal meshes and the foaming of the matrix material.

Acknowledgements

The research presented in this paper was funded by the National Security Subprogramme at the Széchenyi István University (TKP2021-NVA-23).

References

[1] Timeline Of 20th And 21st Century Wars: Imperial War Museum [updated 2024, cited 2024 Mar 5]. Available from: https://www.iwm.org.uk/history/timeline-of-20th-and-21st-century-wars.
[2] Kovács L. The present and possible future of electronic warfare. Hadmérnök. 2017;12(1):213-32.
[3] Csuka A, Előházi J. Directed energy weapons and their hazards to computer systems. Hadmérnök. 2008;3(3):102-11.
[4] TechPro23. EMP Protection: How to Protect Against An EMP Attack [updated 2020, cited 2024 Mar 5]. Available from: https://techprotectbag.com/emp-protection-how-to-protect-against-an-emp-attack/.
[5] Woolsey; RJ, Pry PV. The Growing Threat From an EMP Attack. The Wall Street Journal. 12 Aug 2014.
[6] Electromagnetic Pulse (EMP) Protection and Resilience Guidelines for Critical Infrastructure and Equipment. National Cybersecurity and Communications Integration Center Arlington, Virginia; 2019.
[7] Pereira V, Kunkolienkar GR, editors. EMP (Electro-Magnetic Pulse) weapon technology along with EMP shielding & detection methodology. 2013 Fourth International Conference on Computing, Communications and Networking Technologies (ICCCNT); 2013 Jul 4-6, Tiruchengode, India, doi: 10.1109/ICCCNT.2013.6726651
[8] EMP protection [updated 2018, cited 2024 Mar 5]. Available from: https://hollandshielding.com/en/emp-protection.
[9] Chapman SJ, Hewett DP, Trefethen LN. Mathematics of the Faraday Cage. SIAM Review. 2015;57(3):398-417, doi: 10.1137/140984452.
[10] Klucas G. 'Conductive concrete' shields electronics from EMP attack. Nebraska Today. 2016 Nov 14.
[11] Wang D, Li Y, Dehghanian P, Wang S, editors. Power Grid Resilience to Electromagnetic Pulse (EMP) Disturbances: A Literature Review. 2019 North American Power Symposium (NAPS); 2019 Oct 13-15, Wichita, KS, USA, doi: 10.1109/NAPS46351.2019.9000227.
[12] Kim K, Park Y-J. Development of Decision-Making Factors to Determine EMP Protection Level. Applied Sciences. 2021;11(11):5227, doi: 10.3390/app11115227.
[13] Kim K, Min K-R, Park Y-J. Feasibility Study on the Development of a Deployable Tactical EMP Tent for a Sustainable Military Facility. Sustainability. 2021;13(1):16, doi: 10.3390/su13010016.
[14] Wang Q, Jia D, Pei X, Wu X, Xu F, Wang H, et al. Investigation of Electromagnetic Pulse Compaction on Conducting Graphene/PEKK Composite Powder. Materials. 2021;14(3):636, doi: 10.3390/ma14030636.
[15] Phan DT, Jung CW. Optically transparent and very thin structure against electromagnetic pulse (EMP) using metal mesh and saltwater for shielding windows. Scientific Reports. 2021;11(1):2603, doi: 10.1038/s41598-021-80969-3.
[16] Morales MA, Henry TC, Salamanca-Riba LG. Model of electromagnetic interference shielding effectiveness for a multifunctional composite containing carbon-fiber-reinforced polymer and copper mesh layers. Carbon. 2023;212:118179, doi: 10.1016/j.carbon.2023.118179.
[17] Dogossy G, Kovács JG. Effect of injection moulding pressure on the mechanical properties of ABS. Műanyag És Gumi. 2003;40(9):315.
[18] Jakab SK, Dogossy G. Effect of Injection Molding Parameters on the Chemical Foaming of Acrylonitrile Butadiene Styrene (ABS) Using Breathing Mold Technology. Chemical Engineering Transaction. 2023;107:247, doi: 10.3303/cet23107042.
[19] Jeong E, Kim Y, Hong S, Yoon K, Lee S. Innovative Injection Molding Process for the Fabrication of Woven Fabric Reinforced Thermoplastic Composites. Polymers. 2022;14(8):1577, doi: 10.3390/polym14081577.
[20] Wang J, Mao Q, Jiang N, Chen J. Effects of Injection Molding Parameters on Properties of Insert-Injection Molded Polypropylene Single-Polymer Composites. Polymers. 2022;14(1):23, doi: 10.3390/polym14010023.
[21] Orasugh JT, Ray SS. Functional and Structural Facts of Effective Electromagnetic Interference Shielding Materials: A Review. ACS Omega. 2023;8(9):8134-8158, doi: 10.1021/acsomega.2c05815.
[22] Husaini, Notomi M, Kishimoto K, Shibuya T. Crack Initiation Behavior of ABS Resin Under Mode I and Mixed Mode Loading. Materials Science Research International. 1997;3(3):158-65.
[23] Brzęk P, Sterzyński T. Stress Whitening as an Observation Method of Residual Stress in MABS Polymer Material through the Example of Holding Pressure in an Injection Molding Process. Polymers. 2020;12(12):2871, doi: 10.3390/polym12122871.